

Vector Control of Brushless Doubly-Fed Induction Machines Based on Highly Efficient Nonlinear Controllers

Hamidreza Mosaddegh Hesar , Xiaodong Liang , *Senior Member, IEEE*, Mohammad Ali Salahmanesh, Mojtaba Ayaz Khoshhava , and Salman Abdi

Abstract—Recent advancement in design and control of brushless doubly-fed induction machine (BDFIM) has substantially improved its performance. In this article, two high efficient vector control schemes are proposed for the BDFIM drive based on Lyapunov nonlinear techniques. The first scheme aims for speed control with a one-level structure without an inner loop controller, and the rotor speed error is delivered to a backstepping speed controller. The second scheme has a two-level structure with a backstepping controller and a model reference controller for torque and speed control, respectively. To enhance the performance, the proposed control schemes are based on a novel maximum torque per Ampere (MTPA) control strategy, and their stability is proven by Lyapunov control theory. The proposed controllers are validated experimentally on a 3-kW prototype D132-BDFIM by a TMS320F2833 microcontroller synchronized with a personal computer, and show superior performance over optimal proportional-integral controllers under changing reference speed and load torque.

Index Terms—Backstepping controller, brushless doubly-fed induction machine, Lyapunov control theory, model reference controller, speed control, vector control.

L_{1r}, L_{2r}	Coupling inductances between the stator windings and the rotor.
p	Pole pair number.
f	Frequency.
N_r	Number of nests.
ω	Angular speed.
δ	Current angle.
T_e, T_l	Electromagnetic torque and load torque.
J, B	Moment of inertia and friction coefficient.
K_1, K_2, K_3, K_4, K_5	Controller gains.
a, b	System coefficients.
a_m, b_m	Coefficients of the reference model.
θ_1, θ_2	Adjustable parameters.
<i>Subscripts</i>	
1, 2, r	PW, CW, and rotor.
α, β	Stationary frame axis.
d, q	Rotating frame axis.

NOMENCLATURE

$\vec{V}, \vec{I}, \vec{\lambda}$	Voltage, current, flux vectors.
R	Winding resistance.
L	Winding self-inductance.

I. INTRODUCTION

BRUSHLESS doubly-fed induction machine (BDFIM) is a single frame induction machine with two sets of three-phase windings on its stator. BDFIMs show advantages of doubly-fed induction machines (DFIMs), but with higher reliability due to removing brushes and slip rings from their structure. BDFIMs enable synchronous operation in a wide speed range through frequency control of a control winding (CW), are fault tolerant, and can operate as an induction machine in case of a converter fault. Therefore, BDFIMs have recently attracted significant research interests in various applications, such as variable speed drives [1], [2], wind generators [3], [4], and propulsion systems [5].

Since a BDFIM is not stable in its entire operational speed region, a closed-loop control system is required under dynamic and steady state operations. A number of scalar control methods have been proposed for BDFIMs, such as the phase-angle control [6], open-loop control [7], and closed-loop current control [8]. Due to their relatively slow dynamic responses, these controllers are only suitable for applications such as pumps. In practice, to achieve accurate speed and torque control, BDFIMs require more advanced control structures, such as vector control (VC).

Manuscript received 24 February 2023; revised 4 June 2023 and 4 June 2023; accepted 9 July 2023. This work was supported by the Natural Science and Engineering Research Council of Canada Discovery under Grant RGPIN-2016-04170. (Corresponding author: Xiaodong Liang.)

Hamidreza Mosaddegh Hesar and Xiaodong Liang are with the Department of Electrical and Computer Engineering, University of Saskatchewan, Saskatoon, SK S7N 5A9, Canada (e-mail: pvt356@mail.usask.ca; xil659@mail.usask.ca).

Mohammad Ali Salahmanesh is with the Department of Electrical Engineering, Faculty of Engineering, Ferdowsi University of Mashhad, Mashhad 9177948974, Iran (e-mail: m.salahmanesh@mail.um.ac.ir).

Mojtaba Ayaz Khoshhava is with the Department of Engineering, École de Technologie Supérieure, Montreal, QC H3C 1K3, Canada (e-mail: mojtaba.ayaz-khoshhava@etsmtl.ca).

Salman Abdi is with the School of Engineering, University of East Anglia, NR4 7TJ Norwich, U.K. (e-mail: s.abdi-jalebi@uea.co.uk).

Color versions of one or more figures in this article are available at <https://doi.org/10.1109/TIE.2023.3296811>.

Digital Object Identifier 10.1109/TIE.2023.3296811

A VC system for BDFIMs was first proposed by Oregon State University to control the angle between synchronous frames of the power winding (PW) and CW [9]. However, this traditional multiple reference frames-based method is complex and increases computational burden compared to standard VC schemes. To simplify the control of BDFIMs, a more straightforward derivation of the two-axis model was later proposed by Poza et al. [10]. This unified reference frame model has the same structure as the well-known vector models of conventional induction machines (IMs). Based on this model, a vector controller oriented with the PW flux is proposed in [11], where the feasibility of implementing speed vector control for BDFIMs is discussed, two internal control loops for current control of PW and CW and an external control loop for speed control are designed.

In [12], a vector control method realized in the PW flux reference frame is proposed for a BDFIM operating as a variable speed generator. With this method, the rotor speed and reactive power can be controlled simultaneously through a proportional-integral (PI) controller. In [13], a vector model is developed for the BDFIM with a nested-loop rotor, and vector transformations for the vector model extraction are proposed in a general form such that it can be adapted in various reference frames for different applications. In [14], a vector control system is proposed for BDFIMs using the vector model in [13], and simulation and experimental results are analyzed under various operating conditions. In [15], to cancel the coupling between direct (d) and quadrature (q) channels in vector control, a decoupling matrix is introduced by modeling the BDFIM as a two input-two output system. A model reference observer-based sensorless control system for BDFIMs using errors of CW current is proposed in [16]. The error signal, which is the product of two vectors generated via the reference and adaptive models, is injected to a phase locked loop estimator, and the estimator's output is the estimated rotor position angle. In [16], the observer's stability is proven, dynamic and steady state functionalities are investigated. A proportional-integral-resonant controller-based vector control system for BDFIMs in the grid voltage reference frame is proposed in [17] for wind turbine applications. Tir et al. [18] proposed a fuzzy proportional-integral-derivative (PID) controller for a BDFIM-based variable speed wind energy conversion system. This controller is adaptive with parameters modified online by fuzzy rules.

The maximum torque per Ampere (MTPA) strategy is an effective solution to enhance the machine's efficiency by providing torque with a minimum current magnitude. Extensive research has been done on energy savings using MTPA-based control techniques for singly-fed electric machines in [19], [20], [21], and [22], but only limited studies on efficiency optimization and MTPA have been conducted for the family of brushless doubly-fed machines, especially BDFIMs. In [23], a simple search algorithm based on the microcontroller is introduced to maximize the BDFIM pump drive's efficiency, which can be used to maximize the efficiency of any type of BDFIM variable speed drives. In this algorithm, by choosing the CW's current value, the machine's input power can be minimized under any speed and loading conditions. An analytical method using a core model to maximize the torque-to-current ratio of a BDFIM under

steady state is proposed in [24]. In [25], two control strategies for brushless doubly-fed reluctance machines (BDFRMs) are introduced based on the BDFRM model, the maximum torque per inverter ampere, and the maximum torque per total ampere, intended for variable speed drives. However, in their subsequent studies, only the first strategy's performance was investigated in BDFRM drives [26], [27], [28]. In [29], a search method-based MTPA strategy is proposed for a BDFIM drive, where the total stator current is minimized for a given load torque by a stepwise change of the CW's direct (d)-axis current.

The literature review reveals that there is no inclusive control system for BDFIM drive, which address the concepts of control and efficiency improvement, simultaneously. This article attempts to fill this void by presenting a nonlinear control strategy, which shares the current fairly between the stator windings for a given torque. The novelties of this article are summarized as follows.

- 1) *Two novel control schemes:* BDFIMs experience nonlinear dynamics during operation, which make their control very challenging, and nonlinear control techniques are certainly a suitable choice. Very few works have been done so far in the literature on advanced VC methods, such as nonlinear torque/speed VC, for BDFIMs. To fill in this research gap, in this article, two new vector control algorithms are presented based on nonlinear backstepping controllers. The first control scheme realizes the speed control of a BDFIM through a one-level structure without needing an inner current loop controller. The speed error signals are delivered to the proposed nonlinear backstepping controller. The second control scheme has a two-level structure: an integrator backstepping controller is designed to control the electromagnetic torque; to generate the reference torque, a model reference adaptive controller (MRAC) is designed for the speed loop controller. In MRAC, the desired system operation is defined through a model and control parameters are adjusted based on the error between the model and the closed-loop system.
- 2) *The MTPA control strategy:* To minimize the sum of current magnitudes of PW and CW for a given torque, a MTPA control strategy is developed based on the fifth-order model of the BDFIM, in this article. To guarantee realization of the proposed MTPA, the backstepping speed controller forces the strategy criterion to zero in the first control scheme, where the control outputs are rotor speed and MTPA. In the second control scheme, the deviation from the realization criterion is forced to zero by the backstepping torque controller, and the inputs of this controller are electromagnetic torque and MTPA. To develop the proposed MTPA, a relationship is first obtained for the total stator current versus phase angles of currents of PW and CW. By deriving an auxiliary expression, the phase angle of PW current is then related to the phase angle of CW current, and the total stator current expression is derived using the phase angle of CW current as a controllable variable. Since no straight-forward analytical solution can be obtained for the derivative of this expression, optimal values of the phase angle of

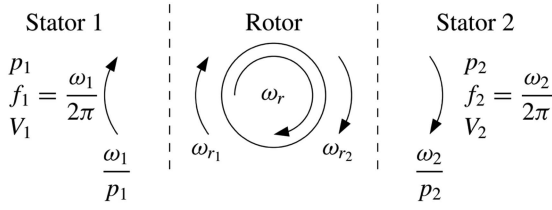


Fig. 1. BDFIM concept: Rotational directions of the main magnetic field components [32].

CW current are calculated by a numerical minimization approach. The proposed method retains all advantages of model-based approaches, such as fast response and high accuracy.

II. BRUSHLESS DOUBLY-FED INDUCTION MACHINES

A. BDFIM Operations

A BDFIM has two three-phase balanced windings on the stator, isolated from each other, one is directly connected to the grid, known as PW, through which most of the power exchange between the grid and the machine occurs. The other winding, known as CW, is connected to the grid through a partially rated converter with a capacity around 35% of the machine's rated power. The rotor of the BDFIM has a special cage structure called nested-loop structure. The number of rotor nests is equal to the sum of pole pairs of PW and CW. Depending on how PW and CW are supplied, a BDFIM may operate in different modes, including induction, cascade, and synchronous modes. Among them, the synchronous mode is the desired mode of operation, in which the voltage amplitude must be adjusted by the power converter based on operating conditions [30]. This mode is ensured when the voltage induced in rotor nested-loops by the PW magnetic field matches the voltage induced by the CW magnetic field. Both magnetic field components induce the same frequency with an equal phase delay between rotor nests [31]. The rotor will then produce two main harmonic rotating field components, coupling with both PW and CW, as shown in Fig. 1. In the synchronous mode, the rotor speed is independent of the applied torque and can be expressed by

$$\omega_r = \frac{\omega_1 + \omega_2}{p_1 + p_2}. \quad (1)$$

If the CW is fed by a dc source ($\omega_2 = 0$), the rotor will rotate at a speed, known as the natural speed [6].

B. BDFIM Vector Model

The fifth-order model of BDFIMs in d-q frame is written by

$$v_{1d} = R_1 i_{1d} + \frac{d\lambda_{1d}}{dt} - \omega_1 \lambda_{1q} \quad (2)$$

$$v_{1q} = R_1 i_{1q} + \frac{d\lambda_{1q}}{dt} + \omega_1 \lambda_{1d} \quad (3)$$

$$v_{2d} = R_2 i_{2d} + \frac{d\lambda_{2d}}{dt} - \omega_2 \lambda_{2q} \quad (4)$$

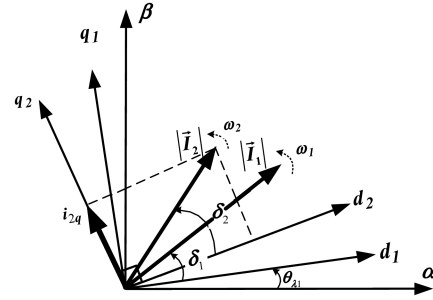


Fig. 2. Current vectors used in equations and their interrelationship.

$$v_{2q} = R_2 i_{2q} + \frac{d\lambda_{2q}}{dt} + \omega_2 \lambda_{2d} \quad (5)$$

$$T_e - T_L = J \frac{d\omega_r}{dt} + B\omega_r. \quad (6)$$

The flux linkages in (2)–(5) are defined as

$$\lambda_{1d} = L_{\sigma 1} i_{1d} + (-L_{\sigma}) i_{2d}, \lambda_{1q} = L_{\sigma 1} i_{1q} - (-L_{\sigma}) i_{2q} \quad (7)$$

$$\lambda_{2d} = (-L_{\sigma}) i_{1d} + L_{\sigma 2} i_{2d}, \lambda_{2q} = -(-L_{\sigma}) i_{1q} + L_{\sigma 2} i_{2q} \quad (8)$$

where $L_{\sigma 1} = L_1 - \frac{L_{1r}^2}{L_r}$, $L_{\sigma 2} = L_2 - \frac{L_{2r}^2}{L_r}$, $L_{\sigma} = \frac{L_{1r} L_{2r}}{L_r}$. The voltage equations of PW and CW are referred to the reference frames rotating at ω_1 and ω_2 , respectively [33].

III. BDFIM CONTROLLER DESIGN

A. MTPA Control Strategy

In this section, an equation for the total stator current against the phase angle of CW current is derived. The total stator current can, then, be minimized for a desired load torque. The electromagnetic torque of a BDFIM can be calculated based on: 1) d - and q -axis components of the CW current and the PW flux linkage, 2) d - and q -axis components of the PW current and the PW linkage flux, and 3) d - and q -axis components of currents of PW and CW

$$T_e = \zeta (\lambda_{1d} i_{2q} + \lambda_{1q} i_{2d}) \quad (9)$$

$$T_e = \xi (\lambda_{1d} i_{1q} - \lambda_{1q} i_{1d}) \quad (10)$$

$$T_e = \eta (i_{1q} i_{2d} + i_{2q} i_{1d}) \quad (11)$$

where $\zeta = \frac{3}{2} (\frac{N_r L_{\sigma 3}}{L_{\sigma 1}})$, $\xi = -\frac{3}{2} N_r$, and $\eta = -\xi L_{\sigma}$. By aligning the d -axis reference frame with the PW flux ($\lambda_{1d} = |\vec{\lambda}_1|$) and considering the relationship between the reference frame positions for PW and CW in Fig. 2 ($i_{1q} = |\vec{I}_1| \sin \delta_1$ and $i_{2q} = |\vec{I}_2| \sin \delta_2$), (9)–(11) can be rewritten, respectively, as

$$T_e = \zeta |\vec{\lambda}_1| |\vec{I}_2| \sin \delta_2 \quad (12)$$

$$T_e = \xi |\vec{\lambda}_1| |\vec{I}_1| \sin \delta_1 \quad (13)$$

$$T_e = \eta |\vec{I}_1| |\vec{I}_2| \sin(\delta_1 + \delta_2). \quad (14)$$

TABLE I

PHASE ANGLES OF CW CURRENT (δ_2) FOR VARIOUS TORQUES UNDER THE PROPOSED CONTROL STRATEGY

	Torque (pu)								
	0.2	0.3	0.4	0.5	0.6	0.7	0.8	0.9	1
δ_2°	31.2	33.1	35.2	36.8	38.1	41.4	44.3	47.1	48.8

By comparing (12) with (14), and (13) with (14), the current magnitudes of PW and CW are obtained in

$$\left| \vec{I}_1 \right| = \frac{\zeta \left| \vec{\lambda}_1 \right| \sin \delta_2}{\eta \sin(\delta_1 + \delta_2)} \quad (15)$$

$$\left| \vec{I}_2 \right| = \frac{\xi \left| \vec{\lambda}_1 \right| \sin \delta_1}{\eta \sin(\delta_1 + \delta_2)}. \quad (16)$$

Accordingly, the total stator current $|\vec{I}_T|$ is expressed by

$$\left| \vec{I}_T \right| = \left| \vec{I}_1 \right| + \left| \vec{I}_2 \right| = \frac{\left| \vec{\lambda}_1 \right| \left(\zeta \frac{\tan \delta_2}{\cos \delta_1} + \xi \frac{\tan \delta_1}{\cos \delta_2} \right)}{\eta (\tan \delta_1 + \tan \delta_2)}. \quad (17)$$

The PW and CW currents are not independent due to the flux and frame alignment conditions. To minimize the total stator current, (17) must be derived in terms of the phase angle of CW current δ_2 . Considering (7) and (10), the relation between phase angles of the currents of PW and CW is determined by

$$\tan \delta_1 = \frac{i_{1q}}{i_{1d}} = \frac{L_{\sigma 1} T_e \tan \delta_2}{\xi \left| \vec{\lambda}_1 \right|^2 \tan \delta_2 - L_{\sigma 1} T_e}. \quad (18)$$

Using (18), $|\vec{I}_T|$ can be determined in terms of δ_2 . By considering $\cos \delta_i = 1/\sqrt{1 + \tan^2 \delta_i}$, ($i = 1, 2$) and substituting (18) in (17), $|\vec{I}_T|$ can be obtained as

$$\left| \vec{I}_T \right| = \frac{\zeta \sqrt{\left(\xi \left| \vec{\lambda}_1 \right|^2 \tan \delta_2 - L_{\sigma 1} T_e \right)^2 + (L_{\sigma 1} T_e \tan \delta_2)^2}}{\eta \xi \left| \vec{\lambda}_1 \right| \tan \delta_2} + \frac{L_{\sigma 1} T_e \sqrt{1 + \tan^2 \delta_2}}{\eta \left| \vec{\lambda}_1 \right| \tan \delta_2}. \quad (19)$$

To determine the minimum value of $|\vec{I}_T|$ for a given torque, the derivative of (19) with respect to $\tan \delta_2$ must be zero. Due to complexity of the derivative equation, no analytical solution exists for this problem. As a result, the optimal value of δ_2 is determined through a numerical minimization method by implementing a function, "fminsearch," in MATLAB. The output of this function is the phase angle of CW current. The variations in the phase angle of CW current for different torques are shown in Table I.

The relationship between d - and q -axis components of the CW current is determined by

$$\tan \delta_2 = i_{2q}/i_{2d} \Rightarrow i_{2d} \tan \delta_2 - i_{2q} = 0. \quad (20)$$

According to (20), the control strategy is realized when $i_{2d} \tan \delta_2 - i_{2q}$ tracks zero as command.

B. Backstepping Torque Controller

In the backstepping approach, nonlinear terms are preserved, and new nonlinear terms are added to the control system as virtual controllers. The Lyapunov stability criteria is used in this control method. By choosing $x_1 = \lambda_{1d}$, $x_2 = i_{2d}$, $x_3 = i_{2q}$, and $x_4 = \omega_r$ as state variables, $U = [u_1 \ u_2]^T$ as the input vector, the affine model is described as follows:

$$\dot{X} = f(x) + g(x)U \quad (21)$$

where

$$f(x) = \begin{bmatrix} v_{1d} - \frac{R_1}{L_{\sigma 1}} x_1 - \frac{R_1 L_{\sigma 2}}{L_{\sigma 1}} x_2 \\ \frac{1}{L_{\sigma 2} - \frac{L_{\sigma 2}^2}{L_{\sigma 1}}} \left(\frac{R_1 L_{\sigma 2}}{L_{\sigma 1}} x_1 - \left(R_2 + \frac{L_{\sigma 2}^2}{L_{\sigma 1}} \right) x_2 \right. \\ \left. - \omega_2 \left(L_{\sigma 2} + \frac{L_{\sigma 2}^2}{L_{\sigma 1}} \right) x_3 - \frac{L_{\sigma 2}}{L_{\sigma 1}} v_{1d} \right) \\ \frac{1}{L_{\sigma 2} + \frac{L_{\sigma 2}^2}{L_{\sigma 1}}} \left(\omega_2 \frac{L_{\sigma 2}}{L_{\sigma 1}} x_1 - \omega_2 \left(L_{\sigma 2} - \frac{L_{\sigma 2}^2}{L_{\sigma 1}} \right) x_2 - R_2 x_3 \right) \\ \frac{1}{J} (T_e - T_L - B \cdot x_5) \end{bmatrix}$$

$$g_1(x) = \begin{bmatrix} 0 \\ \frac{1}{L_{\sigma 2} - \frac{L_{\sigma 2}^2}{L_{\sigma 1}}} \\ 0 \\ 0 \end{bmatrix} \quad g_2(x) = \begin{bmatrix} 0 \\ 0 \\ \frac{1}{L_{\sigma 2} + \frac{L_{\sigma 2}^2}{L_{\sigma 1}}} \\ 0 \end{bmatrix}.$$

The control outputs are defined by

$$\begin{aligned} y_1 &= x_2 \tan \delta_2 - x_3 \\ y_2 &= T_e. \end{aligned} \quad (22)$$

The reference value of the first output is zero. Accordingly, the error dynamics will be

$$\begin{aligned} \dot{e}_1 &= \dot{x}_2 \tan \delta_2 - \dot{x}_3 \\ \dot{e}_2 &= \dot{T}_e - \dot{T}_{ref}. \end{aligned} \quad (23)$$

As a result, we have

$$\begin{bmatrix} \dot{e}_1 \\ \dot{e}_2 \end{bmatrix} = \begin{bmatrix} L_f e_1 \\ L_f e_2 \end{bmatrix} + \begin{bmatrix} L_{g_1} e_1 & L_{g_2} e_1 \\ L_{g_1} e_2 & L_{g_2} e_2 \end{bmatrix} \begin{bmatrix} v_{2d} \\ v_{2q} \end{bmatrix} - \begin{bmatrix} 0 \\ \dot{T}_{ref} \end{bmatrix}. \quad (24)$$

In (24), $L_f e_i$ ($i = 1, 2$) is the Lye derivate of e_i with respect to $f(x)$. To derive the inputs and prove the stability of the control system, the Lyapunov function is determined as follows:

$$V = \frac{1}{2} e_1^2 + \frac{1}{2} e_2^2. \quad (25)$$

The derivative of the Lyapunov function is calculated by

$$\begin{aligned} \dot{V} &= e_1 \dot{e}_1 + e_2 \dot{e}_2 \\ &= e_1 (L_f e_1 + L_{g_1} e_1 v_{2d} + L_{g_2} e_1 v_{2q} \pm K_1 e_1) \\ &\quad + e_2 (L_f e_2 + L_{g_1} e_2 v_{2d} + L_{g_2} e_2 v_{2q} - \dot{T}_{ref} \pm K_2 e_2) \\ &= e_1 (L_f e_1 + L_{g_1} e_1 v_{2d} \pm K_1 e_1) \\ &\quad + e_2 (L_f e_2 + L_{g_2} e_2 v_{2q} - \dot{T}_{ref} \pm K_2 e_2). \end{aligned} \quad (26)$$

To guarantee stability, the derivative of Lyapunov function must be negative definite. Consequently, the control inputs are

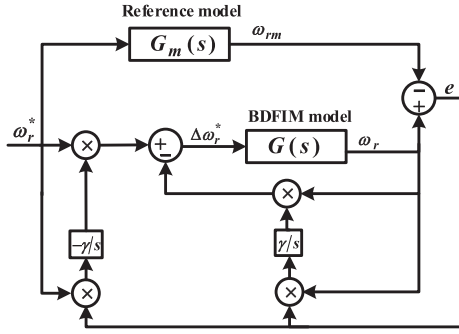


Fig. 3. Block diagram of Lyapunov-based MRAC for the first-order system.

defined as follows:

$$v_{2d} = \frac{1}{L_{g1}e_1} (-L_f e_1 - K_1 e_1) \quad (27)$$

$$v_{2q} = \frac{1}{L_{g2}e_2} (-L_f e_2 - K_2 e_2 + \dot{T}_{ref}). \quad (28)$$

C. Model Reference Adaptive Speed Controller

There is no guarantee for an adaptive controller to result in the closed-loop stability based on the Massachusetts Institute of Technology rule [34]. Accordingly, in this article, the Lyapunov theory has been adapted for the MRAC design. In the first step, a differential equation involving adjustable parameters is derived for the error. Afterward, a Lyapunov function and a tuning mechanism are determined such that the error tends to zero. As the time constant of electrical circuits is much smaller than the mechanical system, a BDFIM can be modeled via the first-order differential equation for the closed-loop speed control through the reference model, as shown in Fig. 3

$$\dot{\omega}_r = -a\omega_r + b\Delta\omega_r^*. \quad (29)$$

To achieve the desired response, the reference model is designated as follows:

$$\dot{\omega}_{rm} = -a_m\omega_{rm} + b_m\omega_r^*. \quad (30)$$

In (30), tuning coefficients of the reference model results in the desired system operation, and the system output follows the output of the reference model. Consistent with Fig. 3, the error is defined as follows:

$$e = \omega_r - \omega_{rm}. \quad (31)$$

The controller is defined by

$$\Delta\omega_r^* = \theta_1\omega_r^* - \theta_2\omega_r. \quad (32)$$

Substituting (29) and (30) in the time differentiate of (31), we have

$$\begin{aligned} \dot{e} = \dot{\omega}_r - \dot{\omega}_{rm} = & -a_m e - (b\theta_2 + a - a_m)\omega_r \\ & + (b\theta_1 - b_m)\omega_r^*. \end{aligned} \quad (33)$$

To derive a tuning mechanism that gives the desired θ_1 and θ_2 , the Lyapunov function is defined as follows:

$$V(e, \theta_1, \theta_2) = \frac{1}{2} \left(e^2 + \frac{1}{b\gamma} (b\theta_1 - b_m)^2 + \frac{1}{b\gamma} (b\theta_2 + a - a_m)^2 \right). \quad (34)$$

In (34), it is assumed that $b\gamma > 0$. As a result, the Lyapunov function is positive definite. To guarantee MRAC's stability, the following criteria must be satisfied:

$$\begin{aligned} \dot{V} & < 0 \forall e \neq 0 \\ \dot{V} & = 0 \forall e = 0. \end{aligned} \quad (35)$$

Consequently, based on (33) and (34), we have

$$\begin{aligned} \dot{V} = e\dot{e} + \frac{1}{\gamma} (b\theta_1 - b_m)\dot{\theta}_1 + \frac{1}{\gamma} (b\theta_2 + a - a_m)\dot{\theta}_2 \\ = -a_m e^2 + \frac{1}{\gamma} (b\theta_1 - b_m) (\dot{\theta}_1 + \gamma\omega_r^* e) \\ + \frac{1}{\gamma} (b\theta_2 + a - a_m) (\dot{\theta}_2 - \gamma\omega_r e). \end{aligned} \quad (36)$$

To satisfy (36), the adaptive law is determined by

$$\dot{\theta}_1 = -\gamma\omega_r^* e \quad \dot{\theta}_2 = \gamma\omega_r e. \quad (37)$$

Consistent with (36) and (37), to proof the asymptotic stability of the closed-loop system, the Barbalat's Lemma [35] is implemented. Thus, the second-order derivative of (36) is determined by considering the adaptive law as follows:

$$\ddot{V} = -2a_m e \dot{e}. \quad (38)$$

From (34) and (36), e is bounded. The reference signal ω_r^* , the output signal of the reference model ω_{rm} , and its first-order derivative are bounded. From (31), the output signal of BDFIM's model ω_r is bounded. From (33), the error derivative is bounded, and thus, (38) is bounded. Based on the Barbalat's Lemma $e \rightarrow 0$, the asymptotic stability is guaranteed.

D. Backstepping Speed Controller

To control the rotor speed directly, another backstepping controller is designed in this section. By choosing $x_1 = i_{1d}$, $x_2 = i_{1q}$, $x_3 = i_{2d}$, $x_4 = i_{2q}$, and $x_5 = \omega_r$ as state variables, the affine model is described by

$$\dot{X} = f(X) + g(X)U \quad (39)$$

where the parameters are defined in (40) shown at the bottom of the next page.

Choosing the control strategy in (20) and the rotor speed as the output variable, tracking errors are introduced as follows:

$$\begin{aligned} e_1 = i_{2d} \tan\delta_2 - i_{2q} = x_3 \tan\delta_2 - x_4 \\ e_2 = \omega_r - \omega_{ref} = x_5 - x_{5ref}. \end{aligned} \quad (41)$$

The error dynamics can be expressed in terms of Lie derivatives by

$$\begin{bmatrix} \dot{e}_1 \\ \dot{e}_2 \end{bmatrix} = \begin{bmatrix} L_f e_1 \\ L_f e_2 \end{bmatrix} + \begin{bmatrix} L_{g1} e_1 & L_{g2} e_1 \\ L_{g1} e_2 & L_{g2} e_2 \end{bmatrix} \begin{bmatrix} v_{2d} \\ v_{2q} \end{bmatrix} - \begin{bmatrix} 0 \\ \dot{\omega}_{ref} \end{bmatrix}. \quad (42)$$

The Lyapunov positive definite function is defined by

$$V_1 = \frac{1}{2} (e_1^2 + e_2^2). \quad (43)$$

The error dynamics in the time derivative of the Lyapunov function candidate can, thus, be derived as follows:

$$\begin{aligned} \dot{V}_1 = & e_1 [L_f e_1 + L_{g_1} e_1 v_{2d} + L_{g_2} e_1 v_{2q} \pm K_3 e_1] \\ & + e_2 \left[\frac{1}{j} \left(-\frac{3}{2} N_r L_\sigma (x_1 x_4 + x_2 x_3) - \frac{T_L}{j} - \frac{B}{j} x_5 \right) \pm K_4 e_2 \right]. \end{aligned} \quad (44)$$

To satisfy the Lyapunov stability criteria, the time derivative of the Lyapunov function must be globally negative definite. The first expression to achieve the control inputs is, thus, obtained from (44) as follows:

$$L_{g_1} e_1 v_{2d} + L_{g_2} e_1 v_{2q} = -K_3 e_1 - L_f e_1. \quad (45)$$

Since the control inputs are not in the second term of (43), a virtual variable is defined as follows:

$$(x_1 x_4)_{ref} = -x_2 x_3 + \frac{2}{3N_r L_\sigma} (-T_L - Bx_5 + jK_4 e_2). \quad (46)$$

In the next step, we try to make $x_1 x_4$ equal to its reference value. Accordingly, the following error signal is defined:

$$e_3 = x_1 x_4 - (x_1 x_4)_{ref}. \quad (47)$$

The error dynamic can be obtained as follows:

$$\dot{e}_3 = L_f e_3 + L_{g_1} e_3 v_{2d} + L_{g_2} e_3 v_{2q} - \frac{d}{dt} (x_1 x_4)_{ref} \quad (48)$$

where, unnumbered eq. shown at the bottom of this page.

The error dynamics equations can be rewritten by

$$\begin{aligned} \dot{e}_1 &= -K_3 e_1 \\ \dot{e}_2 &= -K_4 e_2 + \frac{1}{j} \left(-\frac{3}{2} N_r L_\sigma \right) \\ \dot{e}_3 &= L_f e_3 + L_{g_1} e_3 v_{2d} + L_{g_2} e_3 v_{2q} - \frac{d}{dt} (x_1 x_4)_{ref}. \end{aligned} \quad (49)$$

Since the control inputs are in the third error dynamic, a second Lyapunov function is used to design the final control law as follows:

$$V_2 = \frac{1}{2} (e_1^2 + e_2^2 + e_3^2). \quad (50)$$

Considering the time derivative of the second Lyapunov function, and placing the first to third error dynamics in it, the derivative of this function can be calculated by

$$\begin{aligned} \dot{V}_2 = & e_1 (-K_3 e_1) + e_2 \left(-K_4 e_2 + \frac{1}{j} \left(-\frac{3}{2} N_r L_\sigma \right) e_3 \right) \\ & + e_3 \left[L_f e_3 - \frac{3}{2} N_r L_\sigma \left(\dot{T}_L + jK_4 \dot{e}_2 \right) + Ax_3 + Bx_2 \right. \\ & \left. + \left(L_{g_1} e_3 + \frac{x_3}{\sigma L_\sigma} \right) v_{2d} + \left(L_{g_2} e_3 - \frac{L_{\sigma_1} x_2}{\sigma L_\sigma^2} \right) v_{2q} \pm K_5 e_3 \right]. \end{aligned} \quad (51)$$

$$\begin{aligned} X &= [x_1 \ x_2 \ x_3 \ x_4 \ x_5]^T = [i_{1d} \ i_{1q} \ i_{2d} \ i_{2q} \ \omega_r]^T \\ f(X) &= [f_1 \ f_2 \ f_3 \ f_4 \ f_5]^T = \begin{bmatrix} -\frac{1}{\sigma L_\sigma} \left(\frac{L_{\sigma_2}}{L_\sigma} v_{1d} - \frac{R_1 L_{\sigma_2}}{L_\sigma} x_1 + \omega_2 (L_{\sigma_2} x_4 + L_\sigma x_2) - R_2 x_3 \right) \\ -\frac{1}{\sigma L_\sigma} \left(\frac{L_{\sigma_2}}{L_\sigma} v_{1q} - \frac{R_1 L_{\sigma_2}}{L_\sigma} x_2 + \omega_2 (L_{\sigma_2} x_3 - L_\sigma x_1) + R_2 x_4 - \frac{\omega_1 L_{\sigma_2} |\vec{\lambda}_1|}{L_\sigma} \right) \\ -\frac{1}{\sigma L_\sigma} \left(v_{1d} - R_1 x_1 + \omega_2 L_{\sigma_1} \left(x_2 + \frac{L_{\sigma_2}}{L_\sigma} x_4 \right) - \frac{R_2 L_{\sigma_1}}{L_\sigma} x_3 \right) \\ -\frac{1}{\sigma L_\sigma} \left(-v_{1q} + R_1 x_2 + \omega_2 L_{\sigma_1} \left(x_1 - \frac{L_{\sigma_2}}{L_\sigma} x_3 \right) - \frac{R_2 L_{\sigma_1}}{L_\sigma} x_4 + \omega_1 |\vec{\lambda}_1| \right) \\ \frac{1}{j} (T_e - T_L - Bx_5) \end{bmatrix} \\ g(X) &= [g_1 \ g_2] = \frac{1}{\sigma L_\sigma} \cdot \begin{bmatrix} -1 & 0 & -\frac{L_{\sigma_1}}{L_\sigma} & 0 & 0 \\ 0 & 1 & 0 & -\frac{L_{\sigma_1}}{L_\sigma} & 0 \end{bmatrix}^T, \sigma = 1 - (L_{\sigma_1} L_{\sigma_2} / L_\sigma^2), T_e = -\frac{3}{2} N_r L_\sigma (x_1 x_4 + x_2 x_3) \end{aligned} \quad (40)$$

$$\begin{aligned} & \frac{d}{dt} (x_1 x_4)_{ref} \\ &= \frac{x_3}{\sigma L_\sigma} \underbrace{\left(\frac{L_{\sigma_2}}{L_\sigma} v_{1q} - \frac{R_1 L_{\sigma_2}}{L_\sigma} x_2 + \omega_2 (L_{\sigma_2} x_3 - L_\sigma x_1) + R_2 x_4 - \frac{\omega_1 L_{\sigma_2} |\vec{\lambda}_1|}{L_\sigma} \right)}_A \\ & \quad - \frac{x_3}{\sigma L_\sigma} v_{2d} + \frac{x_2}{\sigma L_\sigma} \underbrace{\left(v_{1d} - R_1 x_1 + \omega_2 L_{\sigma_1} \left(x_2 + \frac{L_{\sigma_2}}{L_\sigma} x_4 \right) - \frac{R_2 L_{\sigma_1}}{L_\sigma} x_3 \right)}_B \\ & \quad + \frac{x_2 L_{\sigma_1}}{\sigma L_\sigma^2} v_{2q} + \frac{2}{3N_r L_\sigma} \left(-\dot{T}_L - jK_4 \dot{e}_2 \right). \end{aligned}$$

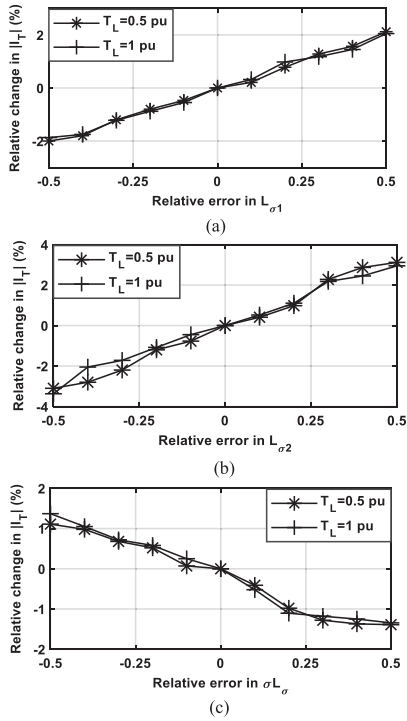


Fig. 4. Relative changes in $|\vec{I}_T|$ versus relative errors in: (a) $L_{\sigma 1}$, (b) $L_{\sigma 2}$, and (c) σL_{σ} .

Through a straightforward calculation, the Lyapunov criterion is satisfied if

$$\begin{aligned} & \left(L_{g1}e_3 + \frac{x_3}{\sigma L_{\sigma}} \right) v_{2d} + \left(L_{g2}e_3 - \frac{L_{\sigma 1}x_2}{\sigma L_{\sigma}^2} \right) v_{2q} = -K_5e_3 \\ & -L_f e_3 + \frac{3}{2}N_r L_{\sigma} \left(\dot{T}_L + jK_4 \dot{e}_2 \right) - Ax_3 - Bx_2 - \frac{3}{2j}N_r L_{\sigma} e_2. \end{aligned} \quad (52)$$

Therefore, we have

$$\dot{V}_2 = -K_3e_1^2 - K_4e_2^2 - K_5e_3^2. \quad (53)$$

Finally, the required voltage space vector is calculated by

$$\begin{aligned} \begin{bmatrix} v_{2d} \\ v_{2q} \end{bmatrix} &= \begin{bmatrix} L_{g1}e_1 & L_{g2}e_1 \\ L_{g1}e_3 + \frac{x_3}{\sigma L_{\sigma}} & L_{g2}e_3 - \frac{L_{\sigma 1}x_2}{\sigma L_{\sigma}^2} \end{bmatrix}^{-1} \\ &\times \begin{bmatrix} -K_3e_1 - L_f e_1 \\ -K_5e_3 - L_f e_3 + \frac{3}{2}N_r L_{\sigma} \left(\dot{T}_L + jK_4 \dot{e}_2 \right) \\ -Ax_3 - Bx_2 - \frac{3}{2j}N_r L_{\sigma} e_2 \end{bmatrix}. \end{aligned} \quad (54)$$

To study the sensitivity of the backstepping speed controller to the motor parameter variations, relative changes in $|\vec{I}_T|$ versus errors in $L_{\sigma 1}$, $L_{\sigma 2}$, and σL_{σ} are shown in Fig. 4. Although the minimum value of $|\vec{I}_T|$ is relatively sensitive to $L_{\sigma 1}$ and $L_{\sigma 2}$, it is insensitive to the error in σL_{σ} in the range of $\pm 25\%$.

IV. EXPERIMENTAL RESULTS AND DISCUSSIONS

The proposed controllers are evaluated through experimental tests. The block diagram of a BDFIM-based drive system is shown in Fig. 5. The experimental setup is shown in Fig. 6,

TABLE II
PARAMETERS OF THE D132 BDFIM PROTOTYPE FOR EXPERIMENTS

Symbol	Value	Symbol	Value
p_1/p_2	2/4	R_r	1.1237 (Ω)
I_1	10 (A)	L_{1r}	0.1863 (H)
I_2	4.5 (A)	L_{2r}	0.0998 (H)
T_e	20 (N.m)	L_{11}	0.0047 (H)
R_1	1.3012 (Ω)	L_{12}	0.0053 (H)
R_2	3.7171 (Ω)	L_{1r}	0.0206 (H)

consisting of a BDFIM coupled to a dc generator, and the control drive system hardware. The DSP-based setup consists of a voltage source inverter with a driver board, a sensor board and a TMS320F28335 signal processor board designed by Texas Instrument Co. for motor control applications with the floating point computation capability, 68 KB RAM and 512 KB ROM. The rotor speed is measured by a 1024 pulses incremental encoder mounted on the BDFIM shaft. The stator phase currents are measured using Hall-effect current sensors and line-to-line voltages are detected by voltage sensors. The measured stator current and voltage signals are filtered by analog second-order low pass filters with a cut-off frequency of 2.6 kHz. The switching frequency should not be lower than half of the sampling frequency [34]. Since the switching frequency is 10 kHz, the sampling frequency is 20 kHz. Table II shows specifications of a 3-kW prototype D132-BDFIM. There are six nests in the rotor, and its natural speed is 500 r/min. This speed is considered as the base value of the per-unit speed. To do the speed control tests, the rotor speed must be first approached to the natural speed. This operating point is obtained by shorting CW through turning on three high-side (or low-side) switches of the power electronic converter. After that, the switches are controlled normally, and the BDFIM operates in the synchronous mode. To evaluate the performance, the test scenario is designed in a way that the proposed control structures can be compared with the vector control algorithm in [11]. To implement this method, the machine flux is kept at the nominal value, the PI speed controller is used, and the load torque increases from 0.4 p.u. to 1 p.u. at a certain time.

Fig. 7(a) shows the total stator current with and without the proposed MTPA control strategy. As expected, the implementation of the MTPA control strategy leads to reduction of $|\vec{I}_T|$, especially under light loads. In Fig. 7(b), the strategy criterion fluctuates around the zero reference, which indicates that the proposed MTPA control strategy is realized. As observed in Fig. 7(c) and (d), by increasing the torque, $|\vec{I}_1|$ is relatively constant, but $|\vec{I}_2|$ is considerably increased. This result is expected because the CW current is responsible for the torque production, and thus, it mostly changes with the torque reference variation. In Fig. 7(e), the speed control results are shown based on three controllers: 1) the backstepping speed controller, 2) the MRAC speed controller, and 3) the optimal conventional PI controller. To make a fair comparison, the PI controller is optimized using the genetic algorithm. The MTPA and speed control loops are optimized under constant $\omega_r = 50\pi/3$ rad/s, and the cost function of the optimization algorithm is defined by

$$F = \int_{t_1}^{t_2} (|\omega_r - \omega_r^*| + |\omega_r^*| \cdot |y|) dt \quad (55)$$

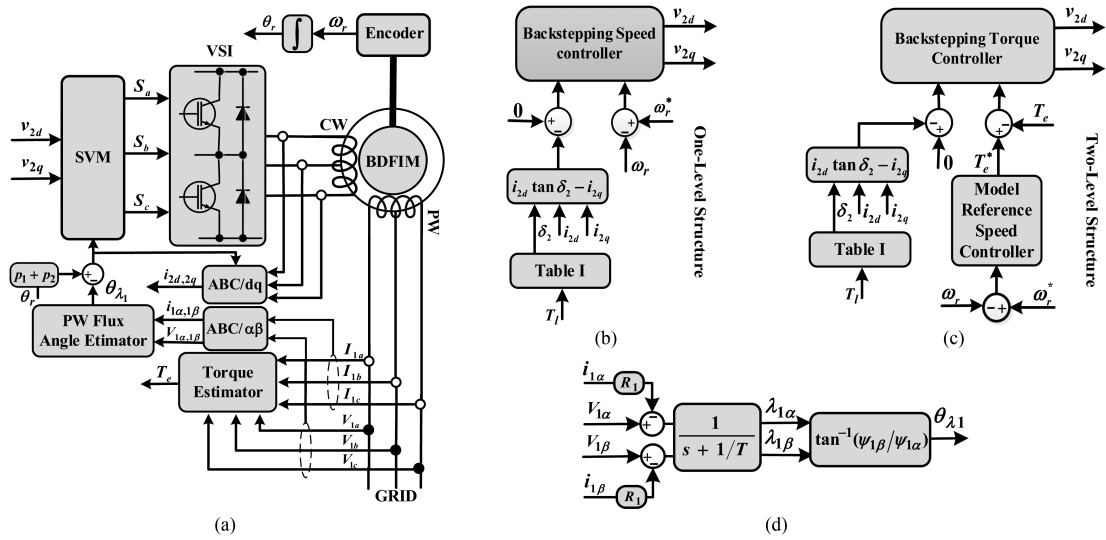


Fig. 5. Block diagrams of a BDFIM drive based on the vector control system. (a) BDFIM-based drive system. (b) One-level structure. (c) Two-level structure. (d) PW flux angle estimator.

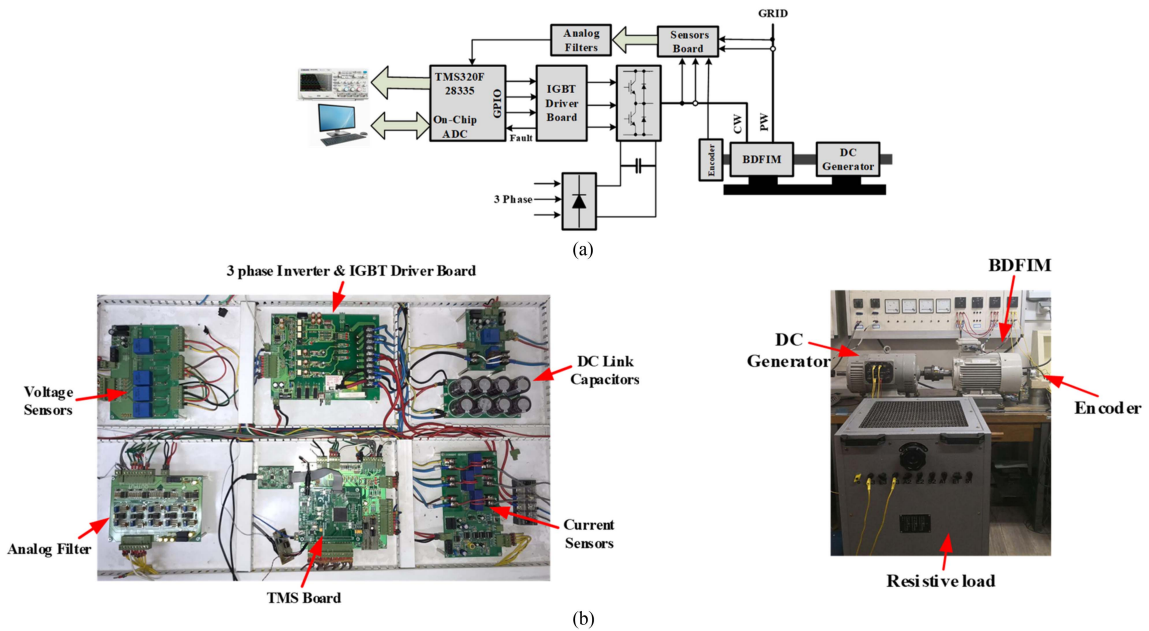


Fig. 6. Experimental setup. (a) Implementation block diagram. (b) BDFIM drive hardware.

where γ is the MTPA realization criterion.

As can be seen, the two proposed controllers are successful in tracking the speed reference immediately after increasing the load torque, however, the PI controller performs unsatisfactorily in terms of settling time. The proposed nonlinear controllers are evaluated under large variations of the rotor speed, i.e., the rotor speed transitions from the subsynchronous zone to the supersynchronous zone. In the test, the load torque remains constant, and the speed reference varies from 0.8 p.u. to 1.2 p.u. exponentially. Fig. 8 shows the control response for the rotor speed reference change. The backstepping speed controller and

the MRAC speed controller perform substantially better than the PI controller in terms of the response speed. Therefore, the proposed nonlinear techniques achieve a stable control of the BDFIM rotor speed. The speed VC results for step changes of the rotor speed reference are shown in Fig. 9, where the load torque remains constant and the rotor speed is increased from the natural synchronous speed to track a step reference. As observed, the dynamic response speed of the drive is significantly improved using the proposed controllers. The values of rise time for the MRAC controller, the backstepping controller, and the PI controller are about 0.84 s, 0.92 s, and 4.77 s, respectively.

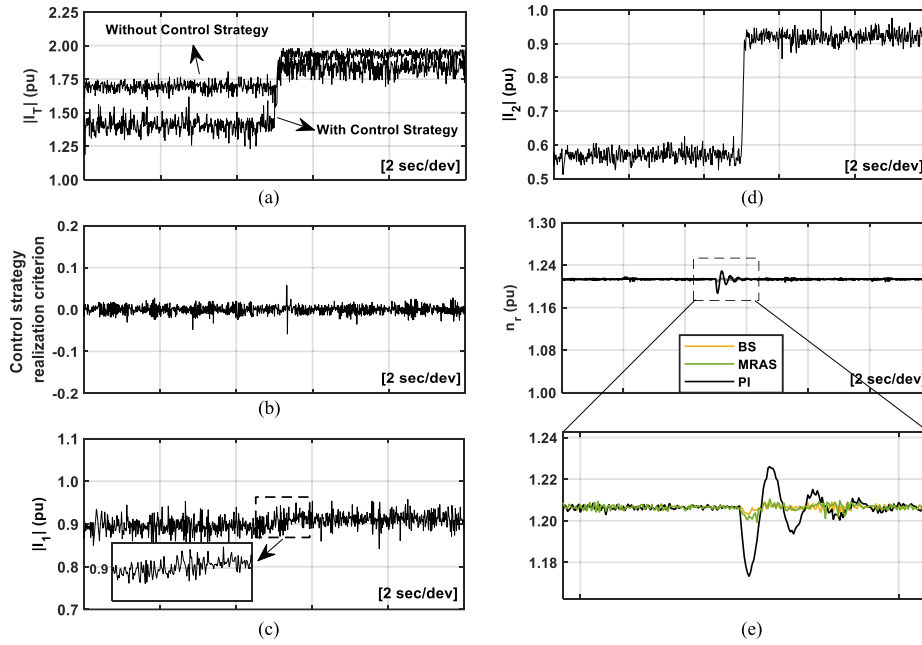


Fig. 7. Experimental results of VC for load changes. (a) Total stator current with and without control strategy. (b) MTPA realization criterion. (c) PW current magnitude. (d) CW current magnitude. (e) Rotor speeds for backstepping (BS) speed controller, MRAC speed controller, and PI controller.

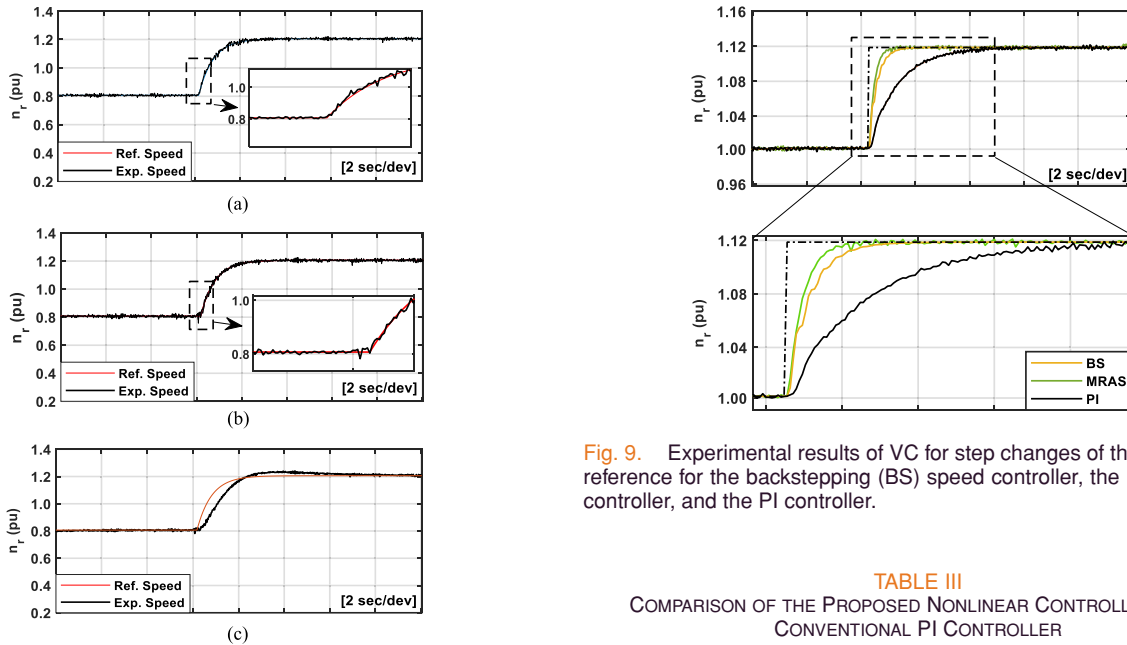


Fig. 8. Experimental results of the VC for large variations in rotor speed. (a) Backstepping speed controller. (b) MRAC speed controller. (c) PI controller.

Table III shows a comprehensive summary of advantages of the proposed controllers over a conventional PI controller. PI controllers provide stability to the system around an equilibrium point. If their parameters (gains of the proportional and integral terms) are not chosen correctly, the controlled process input may become unstable, causing its output diverges. In this context, it

Fig. 9. Experimental results of VC for step changes of the rotor speed reference for the backstepping (BS) speed controller, the MRAC speed controller, and the PI controller.

TABLE III
COMPARISON OF THE PROPOSED NONLINEAR CONTROLLERS AND CONVENTIONAL PI CONTROLLER

The Proposed controllers	The conventional PI controller
Zero steady state errors without under/over-shoot	Zero steady state errors, with under/over-shoot
Fast dynamic response	Slow dynamic response
The total stability of the controller is proven through the Lyapunov theory	The total stability of the PI controller is not proven
Adjustment of three controller gains is required	Adjustment of ten controller gains is required [11]
The d-q cross compensation is not required	The d-q cross compensation is required
Complex structure	Simple structure
Relatively complicated	Easy to use

TABLE IV

COMPARISON OF THE PROPOSED NONLINEAR CONTROLLERS IN THIS ARTICLE AND DIFFERENT VECTOR CONTROL SCHEMES IN THE LITERATURE

Ref.	Type of controller	Control outputs	Operating mode	Dynamic Response	Type of study
[12]	Linear/PI	Speed and reactive power	Generator	Slow	Experimental/Simulation
[13]	Linear/PI	Rotor speed	Generator	Medium	Experimental
[14]	Linear/PI	Rotor speed	Generator	Medium	Experimental
[15]	Linear/PI	Speed and voltage	Generator	Fast	Experimental
[16]	Linear/PI	Speed and current	Generator/Motor	Medium	Experimental
[17]	Linear/PI	Active and reactive power	Generator	Medium	Experimental
[18]	Intelligent/Fuzzy PID	Active and reactive power	Generator	Fast	Simulation
This paper	Nonlinear/Backstepping and MRAS	Rotor speed and torque	Motor	Fast	Experimental/Simulation

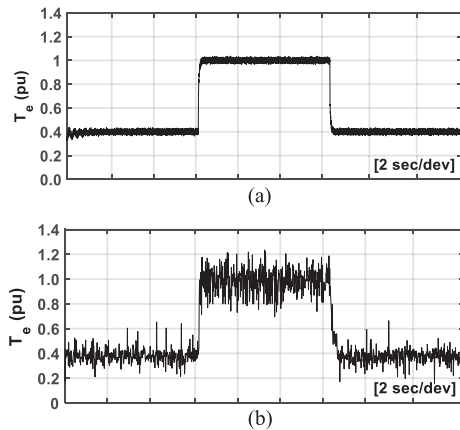


Fig. 10. Electromagnetic torque during transient operations. (a) Simulation result. (b) Experimental result.

is important to know the stability limits of a PI controller in conjunction with the plant, since any variation could provoke instability in the system.

A comparison of the proposed nonlinear controllers in this article and existing methods in the literature for vector control of BDFIMs is shown in Table IV, where their most significant features are summarized.

Waveforms of the electromagnetic torque through simulation and experiments for the two-level structure are shown in Fig. 10. As observed, the electromagnetic torque can properly track the repeating sequence of the load torque between 0.4 p.u. and 1 p.u. A close agreement is observed between the simulation and experimental results. Their difference is due to using the reduced order model for simulation, and the magnetic saturation and iron losses are not considered in the control scheme.

V. COMPARISON OF THE PROPOSED BACKSTEPPING CONTROLLER WITH SOME NONLINEAR CONTROLLERS

Nonlinear controllers have been proposed for BDFIMs in the literature. In [2] and [37], two sliding mode controllers are proposed for BDFIMs for wind turbine and electric drive applications, respectively. The results in [37] illustrate the robustness of this method against parameter variations. Advantages

of the sliding mode controller include simple implementation, disturbance rejection, strong robustness, and fast dynamic responses. However, its stabilization time is not finite and the undesired chattering appears in the controlled states. The comparison between backstepping and sliding mode controllers shows that the backstepping controller can provide a better tracking performance, especially for complex nonlinear systems with high-performance requirements. The back-stepping controller can also handle systems with constraints on control inputs or outputs more effectively than the sliding mode controller. In [38], the decoupling between flux and torque of BDFIMs is achieved through an input–output feedback linearization (IOFL) controller. The IOFL is a technique used to linearize a nonlinear system. The nonlinear system is transformed into a linear system, which can be controlled using standard linear control techniques. Although the IOFL controller is simpler to implement than the backstepping controller, nonlinear terms useful for stability and tracking are removed in the IOFL controller in the process of obtaining control inputs. In the backstepping controller, not only nonlinear terms are not removed, but also new nonlinear terms are added to obtain a better transient performance.

VI. CONCLUSION

In this article, two novel nonlinear control structures of speed control for the BDFIM were proposed based on backstepping and model reference techniques to enhance dynamic performance under load changes and rotor speed variations. The proposed nonlinear controllers show superior performance compared to the conventional linear PI controller. The two proposed control schemes were based on a novel MTPA strategy, leading to a fair current sharing between the two stator windings, and a minimized total stator current for a given torque. Based on experimental results, for load torques equal to 0.4 p.u. and 1 p.u., the reductions of the total current magnitude with MTPA are 11.86% and 4.52%, respectively.

REFERENCES

- [1] H. M. Hesar, X. Liang, H. A. Zarchi, H. Chenarani, and A. Khazaei, "High-efficient nonlinear control for brushless doubly-fed induction machines," *IEEE Trans. Energy Convers.*, vol. 38, no. 2, pp. 1442–1451, Jun. 2023.

- [2] H. Wang et al., "A cascade PI-SMC method for matrix converter-fed BDFIM drives," *IEEE Trans. Transp. Electric.*, vol. 7, no. 4, pp. 2541–2550, Dec. 2021.
- [3] X. Yan and M. Cheng, "A robustness-improved control method based on ST-SMC for cascaded brushless doubly fed induction generator," *IEEE Trans. Ind. Electron.*, vol. 68, no. 8, pp. 7061–7071, Aug. 2021.
- [4] P. Han, M. Cheng, Y. Jiang, and Z. Chen, "Torque/power density optimization of a dual-stator brushless doubly-fed induction generator for wind power application," *IEEE Trans. Ind. Electron.*, vol. 64, no. 12, pp. 9864–9875, Dec. 2017.
- [5] P. Löhdefink, A. Dietz, and A. Möckel, "Direct drive concept for heavy-duty traction applications with the brushless doubly-fed induction machine," in *Proc. IEEE 13th Int. Conf. Ecological Veh. Renewable Energies*, 2018, pp. 1–6.
- [6] S. Shao, E. Abdi, and R. McMahon, "Low-cost variable speed drive based on a brushless doubly-fed motor and a fractional unidirectional converter," *IEEE Trans. Ind. Electron.*, vol. 59, no. 1, pp. 317–325, Jan. 2012.
- [7] D. Feng, P. Roberts, and R. McMahon, "Control study on starting of BDFM," in *Proc. IEEE 41st Int. Universities Power Eng. Conf.*, 2006, pp. 660–664.
- [8] I. Sarasola, J. Poza, E. Oyarbide, and M. A. Rodriguez, "Stability analysis of a brushless doubly-fed machine under closed loop scalar," in *Proc. IEEE 32nd Annu. Conf. Ind. Electron.*, 2006, pp. 1527–1532.
- [9] R. Li, R. Spee, A. K. Wallace, and G. C. Alexander, "Synchronous drive performance of brushless doubly-fed motors," *IEEE Trans. Ind. Appl.*, vol. 30, no. 4, pp. 963–970, Jul./Aug. 1994.
- [10] J. Poza, E. Oyarbide, D. Roye, and M. Rodriguez, "Unified reference frame dq model of the brushless doubly-fed machine," *IEE Electric Power Appl.*, vol. 153, no. 5, pp. 726–734, Sep. 2006.
- [11] J. Poza, E. Oyarbide, I. Sarasola, and M. Rodriguez, "Vector control design and experimental evaluation for the brushless doubly fed machine," *Inst. Eng. Technol. Electric Power Appl.*, vol. 3, no. 4, pp. 247–256, Jul. 2009.
- [12] S. Shao, E. Abdi, F. Barati, and R. McMahon, "Stator-flux-oriented vector control for brushless doubly fed induction generator," *IEEE Trans. Ind. Electron.*, vol. 56, no. 10, pp. 4220–4228, Oct. 2009.
- [13] F. Barati, S. Shao, E. Abdi, H. Oraee, and R. McMahon, "Generalized vector model for the brushless doubly-fed machine with a nested-loop rotor," *IEEE Trans. Ind. Electron.*, vol. 58, no. 6, pp. 2313–2321, Jun. 2011.
- [14] F. Barati, H. Oraee, E. Abdi, S. Shao, and R. McMahon, "The brushless doubly-fed machine vector model in the rotor flux oriented reference frame," in *Proc. IEEE 34th Annu. Conf. Ind. Electron.*, 2008, pp. 1415–1420.
- [15] L. Sun, Y. Chen, J. Su, D. Zhang, L. Peng, and Y. Kang, "Decoupling network design for inner current loops of stand-alone brushless doubly fed induction generation power system," *IEEE Trans. Power Electron.*, vol. 33, no. 2, pp. 957–963, Feb. 2018.
- [16] J. Yang et al., "Sensorless control of brushless doubly fed induction machine using a control winding current MRAS observer," *IEEE Trans. Ind. Electron.*, vol. 66, no. 1, pp. 728–738, Jan. 2019.
- [17] J. Chen, W. Zhang, B. Chen, and Y. Ma, "Improved vector control of brushless doubly fed induction generator under unbalanced grid conditions for offshore wind power generation," *IEEE Trans. Energy Convers.*, vol. 31, no. 1, pp. 293–302, Mar. 2016.
- [18] Z. Tir, O. P. Malik, and M. N. Hashemnia, "Intelligent control of brushless doubly-fed induction generator," *Int. J. Syst. Assurance Eng. Manage.*, vol. 10, no. 3, pp. 326–338, Jun. 2019.
- [19] A. Khazaei, H. A. Zarchi, G. A. Markadeh, and H. M. Hesar, "MTPA strategy for direct torque control of brushless DC motor drive," *IEEE Trans. Ind. Electron.*, vol. 68, no. 8, pp. 6692–6700, Aug. 2021.
- [20] H. R. M. Hesar, H. A. Zarchi, and M. A. Khoshhava, "Online maximum torque per ampere control for induction motor drives considering iron loss using input-output feedback linearisation," *Inst. Eng. Technol. Electric Power Appl.*, vol. 13, no. 12, pp. 2113–2120, Dec. 2019.
- [21] F.-J. Lin, M.-S. Huang, S.-G. Chen, and C.-W. Hsu, "Intelligent maximum torque per ampere tracking control of synchronous reluctance motor using recurrent legendre fuzzy neural network," *IEEE Trans. Power Electron.*, vol. 34, no. 12, pp. 12080–12094, Dec. 2019.
- [22] A. Shinohara, Y. Inoue, S. Morimoto, and M. Sanada, "Direct calculation method of reference flux linkage for maximum torque per ampere control in DTC-based IPMSM drives," *IEEE Trans. Power Electron.*, vol. 32, no. 3, pp. 2114–2122, Mar. 2017.
- [23] B. V. Gorti, G. C. Alexander, R. Spee, and A. K. Wallace, "Microcontroller based efficiency maximization for a brushless doubly-fed machine pump drive," in *Proc. Int. Conf. Ind. Automat. Control*, 1995, pp. 377–381.
- [24] M. Ahmadian, B. Jandaghi, and H. Oraee, "Maximum torque per ampere operation of brushless doubly fed induction machines," *Renewable Energies Power Qual. J.*, vol. 1, no. 9, pp. 981–985, May 2011.
- [25] R. E. Betz and M. G. Jovanovic, "Theoretical analysis of control properties for the brushless doubly fed reluctance machine," *IEEE Trans. Energy Convers.*, vol. 17, no. 3, pp. 332–339, Sep. 2002.
- [26] S. Ademi and M. Jovanović, "Maximum torque per inverter ampere control of brushless doubly-fed reluctance generators for wind turbines," in *Proc. Int. Symp. Power Electron., Elect. Drives, Automat. Motion*, 2014, pp. 883–888.
- [27] S. Ademi and M. G. Jovanović, "Vector control methods for brushless doubly fed reluctance machines," *IEEE Trans. Ind. Electron.*, vol. 62, no. 1, pp. 96–104, Jan. 2015.
- [28] S. Ademi, M. G. Jovanović, H. Chaal, and W. Cao, "A new sensorless speed control scheme for doubly fed reluctance generators," *IEEE Trans. Energy Convers.*, vol. 31, no. 3, pp. 993–1001, Sep. 2016.
- [29] H. Mosaddegh, H. A. Zarchi, and G. A. Markadeh, "Stator flux oriented control of brushless doubly fed induction motor drives based on maximum torque per total ampere strategy," in *Proc. Int. Power Electron., Drive Syst. Technol. Conf.*, 2019, pp. 84–89.
- [30] H. M. Hesar, H. A. Zarchi, and G. A. Markadeh, "Modeling and dynamic performance analysis of brushless doubly fed induction machine considering iron loss," *IEEE Trans. Energy Convers.*, vol. 35, no. 1, pp. 193–202, Mar. 2020.
- [31] U. Shipurkar, T. D. Strous, H. Polinder, J. A. Ferreira, and A. Veltman, "Achieving sensorless control for the brushless doubly fed induction machine," *IEEE Trans. Energy Convers.*, vol. 32, no. 4, pp. 1611–1619, Dec. 2017.
- [32] P. C. Roberts, "A study of brushless doubly fed (Induction) machines," Ph.D. dissertation, Emanuel College, Univ. Cambridge, Cambridge, U.K., Sep. 2004, ch. 1.
- [33] R. E. Betz and M. G. Jovanovic, "Introduction to the space vector modelling of the brushless doubly-fed reluctance machine," *Electric Power Compon. Syst.*, vol. 31, no. 8, pp. 729–755, Jun. 2003.
- [34] K. J. Astrom and B. Wittenmark, *Adaptive Control*, 2nd ed. Addison-Wesley, 1995, ch. 5.
- [35] H. K. Khalil, *Nonlinear Control*, 3rd ed. Prentice Hall, 2002, ch. 8.
- [36] L. Harnefors and H. P. Nee, "Model-based current control of AC machines using the internal model control method," *IEEE Trans. Ind. Appl.*, vol. 34, no. 1, pp. 133–141, Jan./Feb. 1998.
- [37] H. R. M. Hesar and H. A. Zarchi, "Variable structure direct torque control of brushless doubly fed induction generator for wind turbine applications," in *Proc. 22nd Iranian Conf. Elect. Eng.*, 2014, pp. 671–676.
- [38] C. Xia and H. Guo, "Feedback linearization control approach for brushless doubly-fed machine," *Int. J. Precis. Eng. Manuf.*, vol. 16, no. 8, pp. 1699–1709, Jul. 2015.



Hamidreza Mosaddegh Hesar received the M.Sc. and Ph.D. degrees in electrical engineering from Ferdowsi University of Mashhad, Mashhad, Iran, in 2014 and 2019, respectively.

He is currently a Postdoctoral Fellow with Power and Energy Conversion Laboratory, University of Saskatchewan, Saskatoon, Canada. His research interests and activities include control of high-performance drives, modeling of electrical machines, and renewable energy.



Xiaodong Liang (Senior Member, IEEE) was born in Lingyuan, China. She received the B.Eng. and M.Eng. degrees from Shenyang Polytechnic University, Shenyang, China, in 1992 and 1995, respectively, the M.Sc. degree from the University of Saskatchewan, Saskatoon, Canada, in 2004, and the Ph.D. degree from the University of Alberta, Edmonton, Canada, in 2013, all in electrical engineering.

From 1995 to 1999, she was a Lecturer with Northeastern University, Shenyang, China. In 2001, she was Schlumberger (SLB), Edmonton, Canada, and was promoted to a Principal Power Systems Engineer with this world's leading oil field service company in 2009; she was with Schlumberger for almost 12 years until 2013. From 2013 to 2019, she was with Washington State University, Vancouver, WA, United States and Memorial University of Newfoundland in St. John's, NL, Canada as an Assistant Professor and later an Associate Professor. In 2019, she was with the University of Saskatchewan, Saskatoon, Canada, where she is currently a Professor and Canada Research Chair in Technology Solutions for Energy Security in Remote, Northern, and Indigenous Communities. She was an Adjunct Professor with Memorial University of Newfoundland from 2019 to 2022. Her research interests include power systems, renewable energy, and electric machines.

Dr. Liang is the registered Professional Engineer in the province of Saskatchewan, Canada, the Fellow of IET, and the Deputy Editor-in-Chief of IEEE TRANSACTIONS ON INDUSTRY APPLICATIONS.



Mohammad Ali Salahmanesh received the M.Sc. (with honors) degree in electrical engineering in 2019 from Ferdowsi University of Mashhad, Mashhad, Iran, where he is currently working toward the Ph.D. degree in electrical machines and drives.

His research interests include control of electric drives, nonlinear control, modeling of electrical machines, and power electronics.



Mojtaa Ayaz Khoshhava received the M.S. degree from Shiraz University, Shiraz, Iran, in 2014 and the Ph.D. with the Ferdowsi University of Mashhad, Mashhad, Iran, in 2020, both in electrical engineering.

He is currently a Postdoctoral Fellow with École de Technologie Supérieure, Montreal, Canada. His main research interests include electrical machines control, design, and modeling.



Salman Abdi received the B.Sc. degree from Ferdowsi University, Mashhad, Iran, in 2009, the M.Sc. degree from the Sharif University of Technology, Tehran, Iran, in 2011, both in electrical engineering, and the Ph.D. degree in electrical machines design and optimization from Cambridge University, Cambridge, U.K., in 2015.

He is currently an Assistant Professor in electrical engineering with the University of East Anglia, Norwich, U.K. His research interests revolve around electrical machine design, modeling, and instrumentation for renewable power generation and electric propulsion systems.

ing, and instrumentation for renewable power generation and electric propulsion systems.